7th International Symposium on Particle Image Velocimetry
Roma, Italy, September 11-14, 2007

Large Format PIV to Resolve Large and Small Structures Surrounding a Gurney Flap

D. R. Troolin, E.K. Longmire

Abstract A NACA 0015 airfoil with and without a Gurney flap was studied using large format particle image velocimetry (PIV) in order to examine the relation between coherent flow structures upstream and downstream of 1%, 2%, and 4% flaps at Reynolds numbers based on chord length of $Re_c = 0.99 \times 10^5$ and $Re_c = 2.1 \times 10^5$. High spatial resolution PIV over a relatively large field of view revealed the mechanism governing the shedding that occurs in the upstream cavity of the Gurney flap. The dominant vortices upstream of the flap intermittently cause local separations of oppositely rotating fluid. This fluid wraps into smaller opposing vortices that are swept outward and into the freestream by the dominant vortices. The dominant vortices are then pulled outward and convect downstream into the existing Kármán vortex street. This behavior was observed for all flap heights studied.

1 Introduction

Interest in Gurney flaps has increased in the past few years due to their potential utility in high-lift applications in commercial and specialized aircraft. At the same time, recent advances in research capabilities have made more detailed study of such intricate flow devices possible. The Gurney flap is a small tab approximately 1% to 4% of the airfoil chord in length that protrudes typically 90° to the chord at the trailing edge (Fig. 1).

The first use of the flap was on a racecar in the 1970's by Daniel Gurney, for whom it is named. Subsequent studies by Liebeck (1978) and Neuhart and Pendergraft (1988) gave information on the flow structure downstream of the flap. Wind tunnel tests at a Reynolds number of 1.64 x 10^6 on a baseline NACA 4412 were performed by Wadcock in the NASA Ames 7 by 10 foot Wind Tunnel (1987). These tests showed a significant increase in the lift coefficient, shifting the lift curve up by 0.3 for a Gurney flap of 1.25% of the chord length, and providing a higher maximum lift. There was no appreciable increase in drag until the Gurney flap was extended beyond about 2% of the airfoil chord length.

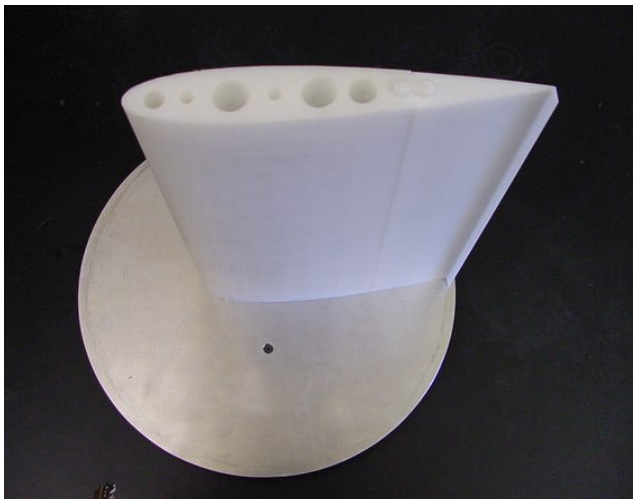

Figure 1: Gurney flap on an airfoil.

Previous studies on the same airfoil configuration using time-resolved PIV have revealed a mode of vortex shedding not previously observed or postulated in experimental or numerical investigations of flow around Gurney flaps (Troolin et al. 2006a). A loosely organized vortex forms and grows in the cavity upstream of the flap until it is expunged into the airfoil wake where it interacts with the Kármán vortex street that forms directly downstream of the flap. This upstream vortex shedding was not present in a case with a "filled-in" flap that generated approximately half the lift increment of the open-cavity case. Thus, it appears that a significant part of the lift increment produced by the Gurney flap results directly from the upstream shedding and its influence on the trailing wake.

In addition, the two shedding modes of different frequency interact downstream of the flap to generate constructive or destructive interference depending on the phases during which they merge. In all cases, these interactions served to increase the downward velocity in the airfoil wake, and thus the circulation and lift, as compared to the closed flap case.

The different flap heights displayed very similar wake and shedding interference patterns, with the coherent structures in each scaling approximately with the height of the flap. For example, Strouhal numbers $St = hf/U$ associated with the primary and secondary shedding modes at $\alpha = 8°$ were (0.17, 0.14) and (0.16, 0.13) for the 4%

D. R. Troolin, TSI Incorporated, 500 Cardigan Road, Shoreview, MN 55126, USA
E. K. Longmire, Department of Aerospace Engineering and Mechanics, University of Minnesota, Minneapolis, MN 55455, USA

and 2% flaps respectively. Also, the ratio of primary to secondary shedding modes was found to be nearly constant at approximately 0.8 for the 4% and 2% flap configurations. Thus, these preliminary results suggest that perhaps the shedding mode ratio is independent of the Gurney flap height, as long as coherent shedding modes exist (Troolin et al. 2006b).

The aim of this study was to couple the knowledge gained from the more coarsely resolved high speed PIV measurements of previous studies, with the current large format, high resolution PIV measurements. An 11 million pixel camera at a magnification of nearly 1:1 was used to capture instantaneous velocity fields displaying the spatial interaction of the vortex shedding both upstream and downstream of the Gurney flap. While it is known that multiple shedding modes exist in the region of the Gurney flap, the precise mechanisms which govern the upstream shedding has not been determined. The following data reveals the nature of this shedding, and the events which lead up to, and cause, the sudden downsurge that is the catalyst for the increased lift generated by the Gurney flap.

2 Experimental Apparatus

The experiments were conducted in the University of Minnesota Aerospace Engineering Open Return Wind Tunnel. The test section is 0.6 m × 0.6 m in cross section, and hot-film anemometry measurements show a freestream turbulence intensity of less than 0.25%. The airfoil section had a wing span (b) of 304.8 mm and a chord length (c) of 190.5 mm, resulting in an aspect ratio of A = 0.49. The airfoils and flap attachments were made in a rapid prototype machine at the University of Minnesota Department of Aerospace Engineering and Mechanics. The airfoil was mounted to a flat, circular, aluminum plate and was then mounted to the wind tunnel sting, with the free end close (~ 2 mm) to the wind tunnel side wall. This served to simulate the effect of an infinite aspect ratio, since the 3D effects at the wingtips were minimized. Four Gurney flap configurations were tested on a symmetric NACA0015 airfoil, 0% (no Gurney flap), 1%, 2%, and 4%, where the height of the Gurney flap is measured relative to the airfoil chord length. Flow visualization with tufts and PIV measurements were performed at two Reynolds numbers based on chord length of $Re_c = 0.99 \times 10^5$ and $Re_c = 2.1 \times 10^5$, where the freestream velocity for these cases was 7.97 m/s and 17.1 m/s respectively. For the flow visualization, tufts were glued to one side of the airfoil at regular intervals of approximately 20 mm. The tufts were made of fine white thread with a length of approximately 25 mm (Fig. 2).

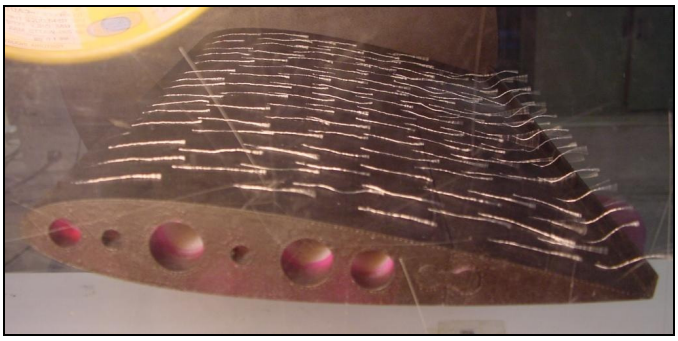

Figure 2: Airfoil section with tufts mounted in wind tunnel.

The PIV measurements were made with the laser light sheet entering the wind tunnel from above. For this reason, the airfoil was inverted so that the area in the upstream cavity of the Gurney flap could be imaged. The camera was located on the side of the tunnel. The data from the PIV configuration has been inverted in the subsequent plots for purposes of comparison. A dual-head Nd:YAG laser emitted 120 mJ/pulse at a wavelength of 532 nm. A -25 mm cylindrical and a 500 mm spherical lens were used to transform the circular laser beam into a sheet. The light sheet thickness was estimated to be 750 μm as determined through the use of laser burn paper. Digital image sequences were acquired from a 12-bit CCD camera at a rate of 1 fps (0.5 Hz PIV capture rate). The resolution of the camera was 4008 × 2672 pixels, with an individual pixel size of 9 μm. A 105 mm lens at f# 5.6 was used along with two 14 mm extension rings to provide a very high magnification ratio of nearly 1:1. For this reason, the field of view was approximately the same as the CCD size (36.07 × 24.05 mm). The time between laser pulses was 5 μs, which allowed for a maximum particle displacement of 7-8 pixels at U_∞. The airflow was seeded with 1μm atomized olive oil droplets generated by a Laskin nozzle. In order to reduce laser reflection from the airfoil surface, rhodamine B paint was applied to the airfoil, and a 532 ± 10 nm bandpass filter was attached to the camera lens. The rhodamine paint is excited by the 532nm (green) laser light and emits between 560 nm and 600 nm (orange) light, which was filtered out by the camera filter. The PIV setup, as well as the effect of the rhodamine B paint can be seen in Fig. 3.

D. R. Troolin, TSI Incorporated, 500 Cardigan Road, Shoreview, MN 55126, USA
E. K. Longmire, Department of Aerospace Engineering and Mechanics, University of Minnesota, Minneapolis, MN 55455, USA

For each run, 50 PIV velocity fields were captured. The vector fields were determined using a CDIC deformation algorithm described by Wereley and Gui (2001). This four-pass method used an interrogation region of 32 by 32 pixels with 75% overlap, which corresponds to a spatial resolution of between 320 and 360 μm depending on the exact magnification, which varied slightly for each case. The first two passes consisted of a recursive grid to determine integer pixel displacement values. The following two passes employed the four-corner deformation grid. This processing scheme provided 99% or higher valid vectors.

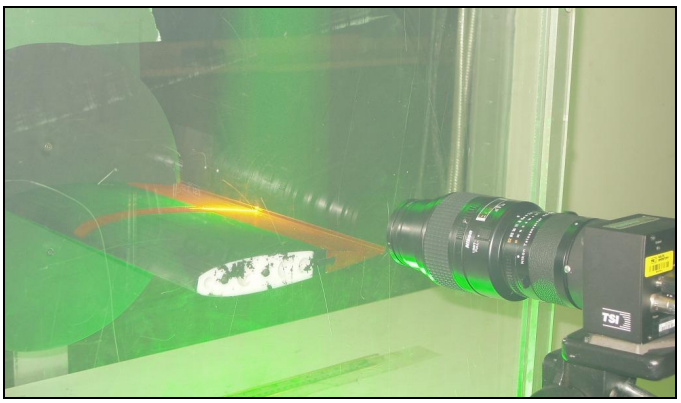

Figure 3: PIV experimental setup in wind tunnel.

3 Results

Tuft Flow Visualization

Tufts of fine white thread were glued to the airfoil surface in order to provide a qualitative measure of the location of the trailing edge separation point for various Reynolds numbers and angles of attack. Since the Gurney flaps could be installed in either direction relative to the tufted surface, both the pressure and suction surfaces of the airfoil could be visualized. Two Reynolds numbers were considered: $Re_c = 0.99 \times 10^5$ and $Re_c = 2.1 \times 10^5$, and the angle of attack was varied from $\alpha = 0°$ up to and including the angle of full-stall, in increments of 1°. The presence of the Gurney flap on the NACA0015 did not change the angle of attack at which flow stalled on the suction surface with this resolution. At the low Reynolds number ($Re_c = 0.99 \times 10^5$), the airfoil stalled at $\alpha = 14°$, and at the high Reynolds number ($Re_c = 2.1 \times 10^5$), the stall occurred at $\alpha = 17°$. An interesting phenomenon was seen on the pressure surface of the airfoil as the angle of attack was increased. As expected, no separation was observed on the pressure surface for the no-flap case. By contrast, the separation zone upstream of the 4% Gurney flap increased in size with increasing angle of attack. Figure 4 shows the pressure surface for the 4% flap at $Re_c = 0.99 \times 10^5$ for $\alpha = 0°$ and $\alpha = 8°$. The red dashed line indicates the approximate location of the boundary between attached and separated flow. This trend was confirmed based upon multiple observations of this effect.

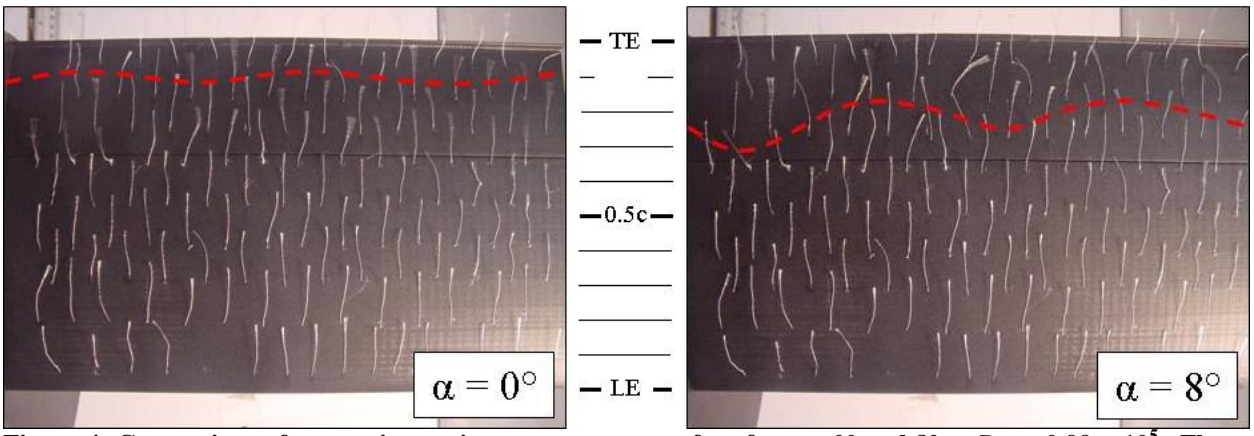

Figure 4: Comparison of separation regions on pressure surface for $\alpha = 0°$ and 8° at $Re_c = 0.99 \times 10^5$. Flow moves bottom to top.

Ensemble-Averaged PIV Measurements

Contours of time-averaged streamwise velocity overlaid with streamlines are presented in Figs. 5 and 6 for 4% and 2% Gurney flaps at both Reynolds numbers for $\alpha = 0°$ and $\alpha = 8°$. Results from fifty independent fields were averaged to obtain the plots which are normalized by the freestream velocity U_∞. Every tenth vector is shown in the horizontal direction, and every other vector is shown in the vertical direction. The area shown in white is the airfoil,

D. R. Troolin, TSI Incorporated, 500 Cardigan Road, Shoreview, MN 55126, USA
E. K. Longmire, Department of Aerospace Engineering and Mechanics, University of Minnesota, Minneapolis, MN 55455, USA

and no data were obtained in the gray areas which were blocked from the illuminating laser light. The shape of the streamlines in the downstream wake closely matches those that were captured with the more coarsely resolved high-speed PIV (Troolin et al. 2006a).

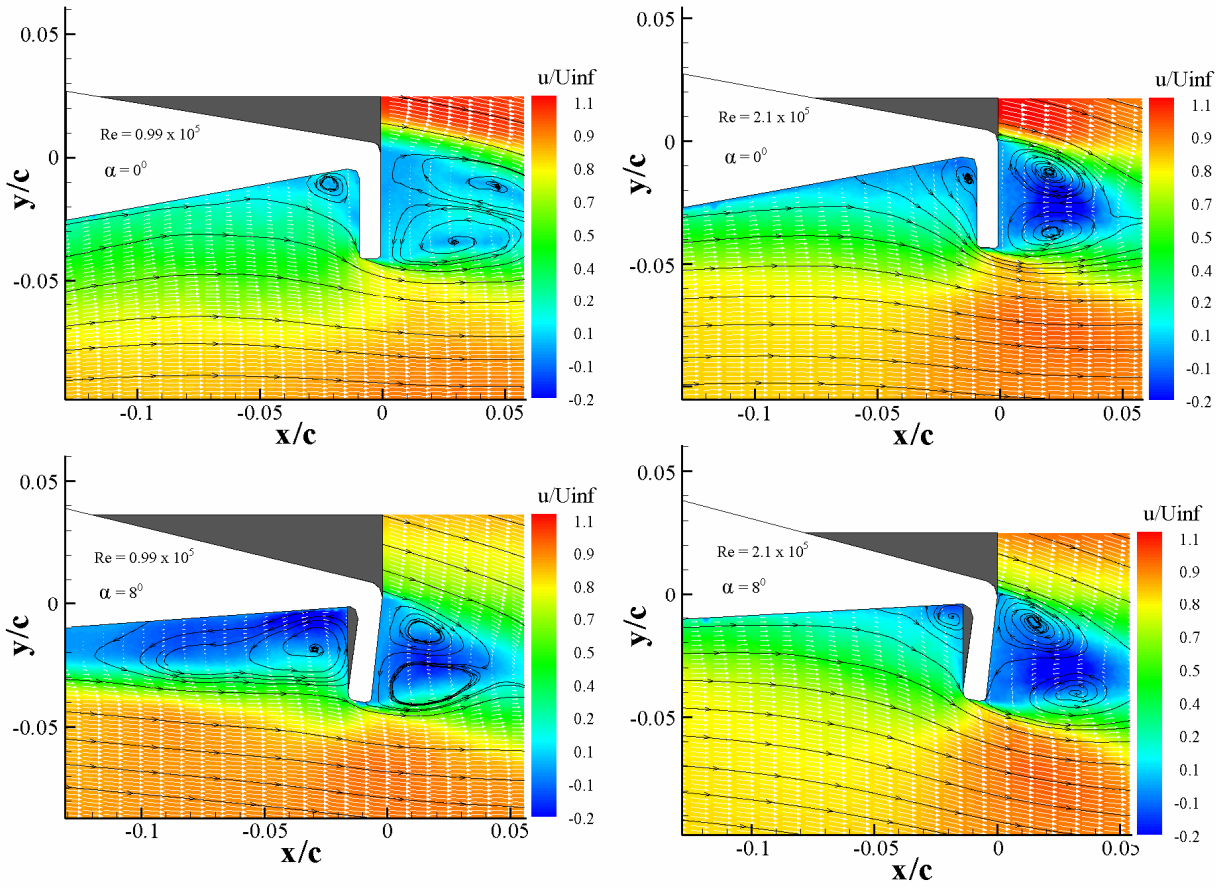

Figure 5: Average of 50 PIV fields at $Re_c = 0.99 \times 10^5$ (left) and $Re_c = 2.1 \times 10^5$ (right) for the 4% Gurney flap at α = 0° (top) and α = 8° (bottom). Color contours represent normalized streamwise velocity.

Three trends can be noted from the plots. First, the area of decreased streamwise velocity directly upstream of the Gurney flap increases in length as the angle of attack increases from α = 0° to α = 8°. This trend, which is consistent with the tuft visualization results, is very clear for the lower Re case (left) but less clear for the higher Re case (right). Second, the average separated zone upstream of the flap decreases in size with increasing Reynolds number, particularly at α = 8°. Third, the zone of recirculating fluid *downstream of the flap* decreases in streamwise length as the angle of attack is increased for $Re_c = 0.99 \times 10^5$ (left), and increases in length for $Re_c = 2.1 \times 10^5$ (right). This is directly related to the upstream recirculation zone. For the lower Reynolds number case, the upstream recirculation zone is much longer so that the streamlines outside this zone are straight and directed nearly parallel to the chordline. The streamlines are drawn easily into the downstream wake leading to a shorter recirculation zone. By contrast, in the higher Reynolds number case, the streamlines outside the upstream recirculation zone are diverted strongly by the flap so that they are directed downward as they pass the flap. They then undergo far greater curvature downstream of the flap before closing off the downstream recirculation zone. The shorter downstream recirculation zone seen in Figs. 5 and 6 for α = 8° and $Re_c = 0.99 \times 10^5$ is associated with increased downward curvature of the suction-side streamlines, which must result in a net increase in the circulation. Tests performed at $Re_c = 2.1 \times 10^5$ on an identical airfoil with the upstream cavity filled-in revealed less benefit in terms of the increase in lift (Troolin et al. 2006a). Neuhart and Pendergraft (1988) found similar results for a different airfoil geometry at $Re_c = 8588$. This suggests that the existence of greater streamline curvature around the Gurney flap on the pressure side of the airfoil may be a key factor in the increased lift.

D. R. Troolin, TSI Incorporated, 500 Cardigan Road, Shoreview, MN 55126, USA
E. K. Longmire, Department of Aerospace Engineering and Mechanics, University of Minnesota, Minneapolis, MN 55455, USA

Plots of the averaged velocity fields for the 2% flap are shown in Fig. 6. It is interesting to note that the trends are consistent between the 4% and 2% flap cases. (The same trends are also observable in averaged velocity fields of the 1% flap case). In contrast to the 4% case, where the flap length is large compared to the unperturbed boundary layer thickness, the two smaller flaps have length more comparable to the thickness, as determined using Blake's (1986) estimate of displacement thickness for blunt trailing edges, and are more relevant to practical applications. As Wadcock (1987) determined previously for higher Reynolds numbers (and therefore thinner boundary layers), Gurney flaps did not cause appreciable increases in drag until they extended beyond about 2% of the chord length.

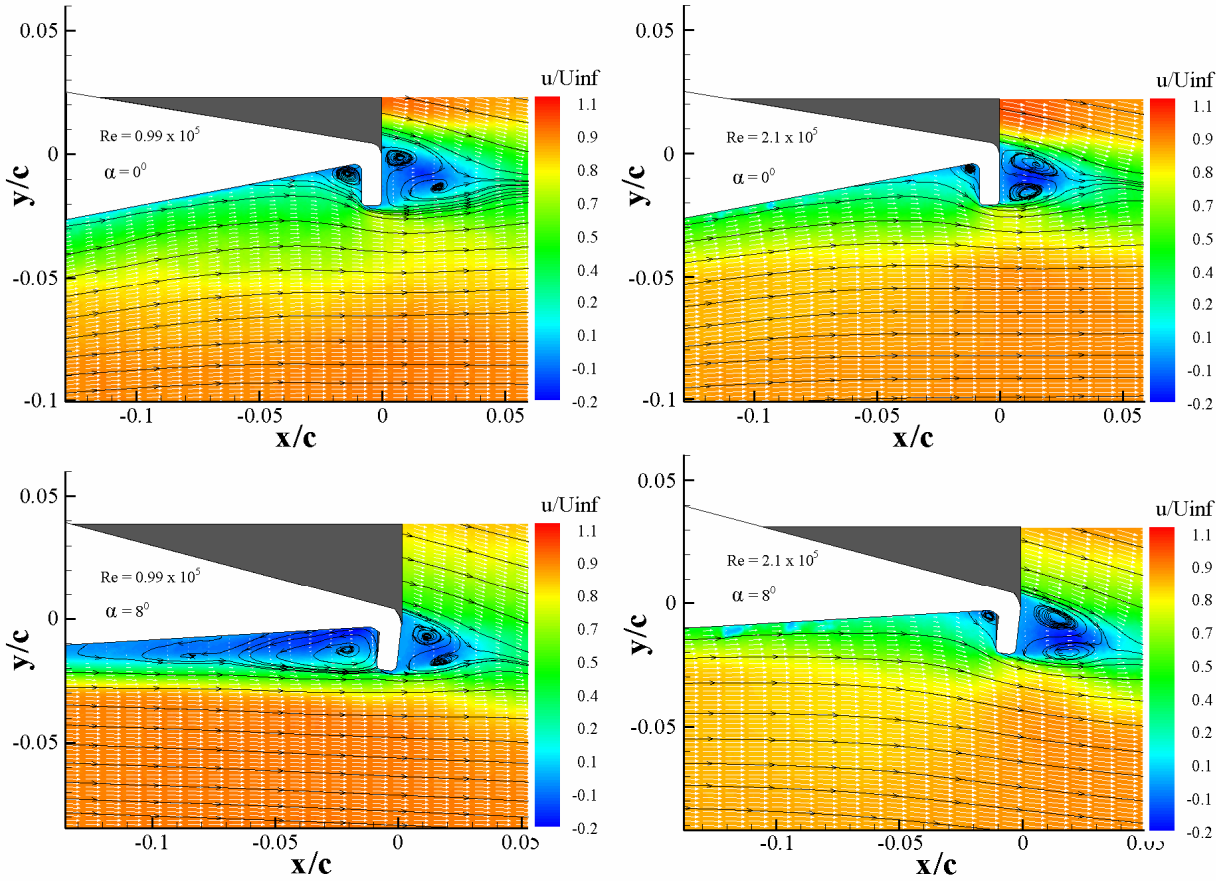

Figure 6: Average of 50 PIV fields at Re_c = 0.99 × 10^5 (left) and Re_c = 2.1 x 10^5 (right) for the 2% Gurney flap at α = 0° (top) and α = 8° (bottom). Color contours represent normalized streamwise velocity.

Instantaneous PIV Measurements

The instantaneous large format PIV measurements were very valuable in understanding, with high spatial resolution, the nature of the vortex shedding from the upstream cavity. Based on time-resolved PIV from previous work, the mechanisms by which slow-moving fluid is ejected from the upstream cavity are well characterized, however, the small structures of the flow (particularly in the region of the upstream cavity), have not previously been resolved in the context of the larger structures. Figure 7 consists of a nominal sequence of instantaneous PIV velocity fields. Streamlines are plotted over the normalized vorticity ($\omega c/U_\infty$) for the case of the 2% Gurney flap at Re_c = 0.99 × 10^5 and α = 0°. The red regions indicate areas of positive or counterclockwise vorticity, while blue indicates areas of negative or clockwise vorticity. Though the current measurements were not time-resolved, the pattern of large flow structures is known and well documented from previous time-resolved work, and this reconstructed sequence represents a typical upstream shedding event.

D. R. Troolin, TSI Incorporated, 500 Cardigan Road, Shoreview, MN 55126, USA
E. K. Longmire, Department of Aerospace Engineering and Mechanics, University of Minnesota, Minneapolis, MN 55455, USA

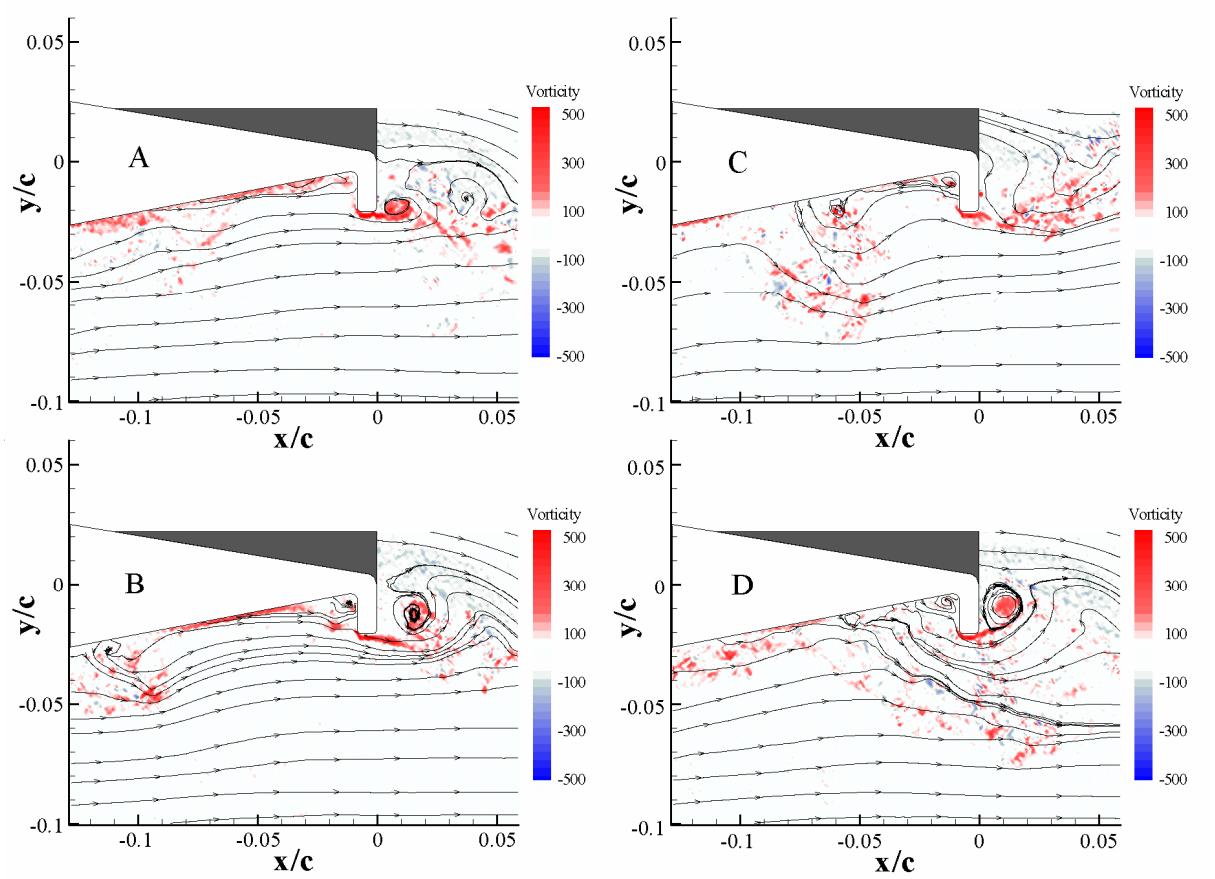

Figure 7: Nominal sequence of instantaneous normalized vorticity fields with streamlines for the 2% Gurney flap at $Re_c = 0.99 \times 10^5$ and $\alpha = 0°$.

Due to the presence of the Gurney flap, there exists a region of separated flow located in the upstream cavity of the flap. The following sequence of events will be described according to Fig. 7, though it should be noted that the starting point of this sequence is arbitrary and chosen simply to aid in the description of the shedding mechanism. In Fig. 7A, there is little large scale activity in the upstream cavity. Figure 7B reveals a small positive vortex forming directly upstream of the flap, and another positive vortex far upstream of the flap that is being convected downstream along the airfoil surface. Figure 7C shows the upstream vortex approaching the vortex in the cavity. Note the regions of largely diffuse positive vorticity spreading downward from the upstream vortex; plots of two-dimensional swirl (not shown) indicate the presence of vortex cores normal to the plane within this region, which are not revealed by the streamlines. In the final plot (Fig. 7D), the vortices merge and the large region of positive vorticity is shed from the airfoil surface and drawn into the downstream wake where interactions with the vortex street subsequently occur.

Figure 8 outlines the sequence with the airfoil at $\alpha = 8°$. As was seen in the earlier figures, the average upstream recirculation zone is much larger for this case, and thus, the vortex interactions are seen more clearly. In Fig. 8A, two large positive (red) vortices are located in the cavity upstream of the flap. The downstream vortex generates negative (blue) vorticity close to the airfoil surface. The location and action of the zone of negative vorticity are key identifiers in determining the timing of an upstream shedding event. As the downstream portion of the larger positive vortex impinges on the upstream face of the flap, it becomes trapped, in the sense that the flap prohibits its convection downstream (Fig. 8B). Vortices further upstream continue to convect toward the trapped vortex, compressing it spatially. Since the circulation encompassing this vortex remains nearly constant, the rotational velocity increases. At a critical point, the rotational velocity of the trapped vortex is sufficient to generate a local separation, dragging the zone with negative vorticity out into the freestream. This can be seen clearly in Fig. 8C

D. R. Troolin, TSI Incorporated, 500 Cardigan Road, Shoreview, MN 55126, USA
E. K. Longmire, Department of Aerospace Engineering and Mechanics, University of Minnesota, Minneapolis, MN 55455, USA

where the blue shear layer peels away from the airfoil surface and a negative (blue) vortex develops. As this blue vortex is dragged into the area near the freestream, it is quickly propelled downstream, which serves to then drag the large trapped positive vortex out of the upstream cavity, which can be seen as the large patch of red directly below and to the right of the Gurney flap in Fig. 8D. With this, the spatially significant "ejection" occurs, which is the most obvious part of the upstream shedding that was observed previously in the time-resolved PIV fields. The ejected structures subsequently interact with the asymmetric Kármán vortex street which exists in the downstream wake, and the progression repeats. If the ejection coincides with a similar-signed streamwise normal (downward) velocity surge in the vortex street, the structures interfere with each other positively, creating an even larger downward surge. Conversely, if the ejection occurs during a momentary upsurge in the downstream vortex street, the two events interfere negatively, potentially "canceling each other out." Since the two shedding modes are not closely coupled, any manner of downstream interaction between these two extremes can occur.

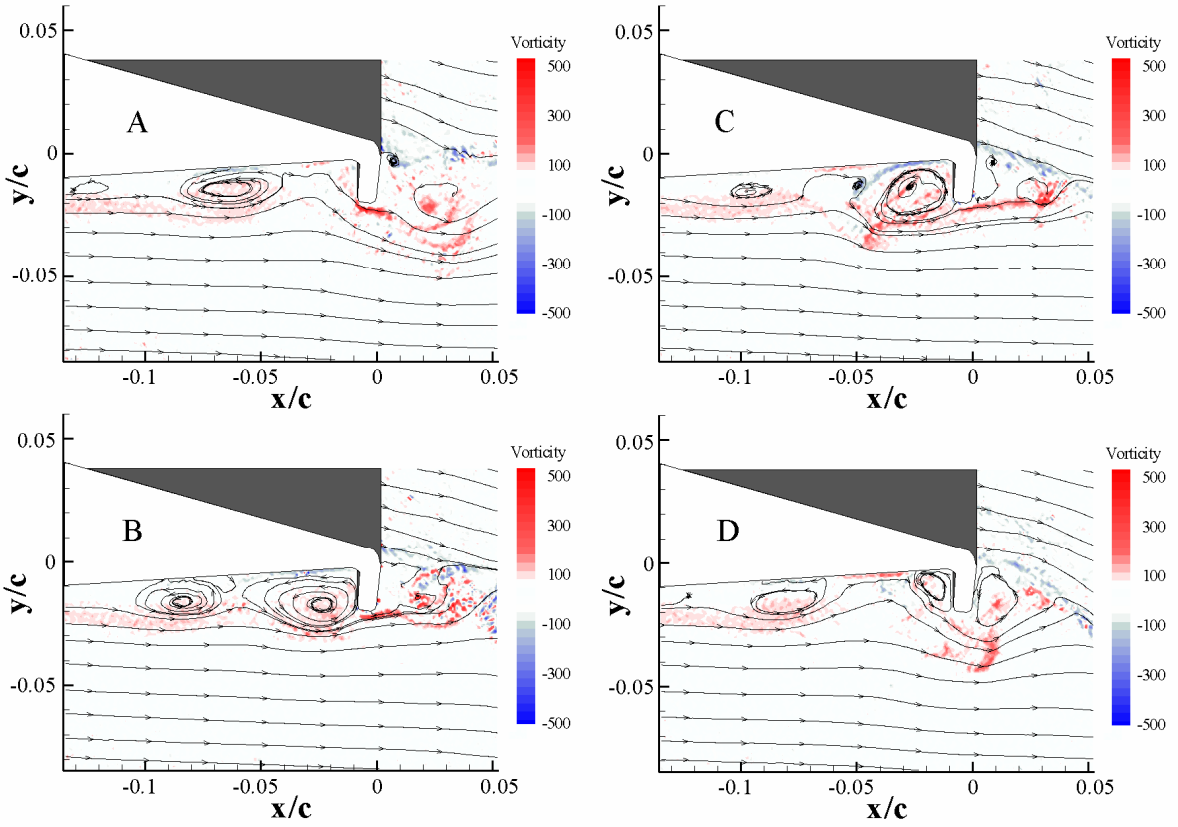

Figure 8: Nominal sequence of instantaneous normalized vorticity fields with streamlines for the 2% Gurney flap at $Re_c = 0.99 \times 10^5$ and $\alpha = 8°$.

Figure 9 represents a similar sequence as Fig. 8 at the higher Reynolds number of $Re_c = 2.1 \times 10^5$. The most obvious difference between this and the previous two figures is the smaller size of the upstream recirculation zone. In addition, the regions of significant vorticity are focused closer to the airfoil surface as expected for the higher freestream velocity and Reynolds number. Figure 9A begins with little activity in the upstream cavity. Progressing to Fig. 9B, a positive vortex is seen to form upstream of and adjacent to the flap. Figure 9C reveals that a second positive vortex has formed upstream of the first, and the two begin to interact. Finally, in Fig. 9D, the two vortices have merged and been drawn into the downstream wake to interact with the trailing vortex street.

D. R. Troolin, TSI Incorporated, 500 Cardigan Road, Shoreview, MN 55126, USA
E. K. Longmire, Department of Aerospace Engineering and Mechanics, University of Minnesota, Minneapolis, MN 55455, USA

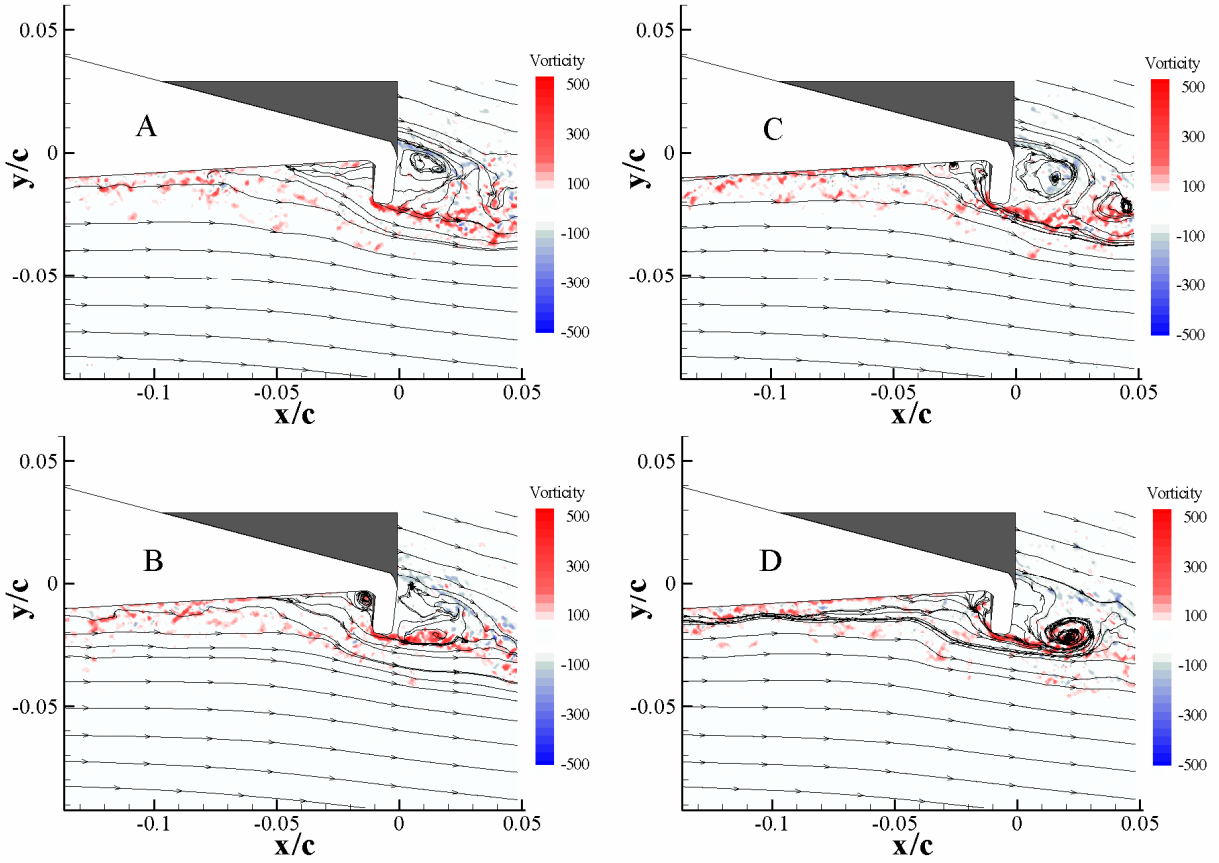

Figure 9: Nominal sequence of instantaneous normalized vorticity fields with streamlines for the 2% Gurney flap at $Re_c = 2.1 \times 10^5$ and $\alpha = 8°$.

4 Conclusions

The preceding work has provided finely resolved details of the vortex interactions upstream of a Gurney flap. A recirculation zone exists upstream of the flap that is large at lower Reynolds numbers, and decreases in size as the Reynolds number is increased. As the angle of attack is increased, the upstream recirculation zone also increases in size.

Within the upstream recirculation zone, positive coherent vortices are convected from upstream toward the forward face of the flap. As a large positive vortex encroaches on the flap, it becomes compressed, and the rotational velocity increases. This causes a local separation when a region of negative boundary layer vorticity between the positive vortex and the airfoil surface is pulled outward toward and eventually into the freestream. This in turn causes the positive vortex to be dragged into the freestream as well. The structures are then convected into the downstream wake where they interact with the downstream Kármán vortex street.

This study was unique in its ability to provide high spatial resolution over a large area. An 11 million pixel camera captured an area of 36 mm × 24 mm, resulting in a velocity spatial resolution of between 320 and 360 µm. This high magnification made it possible to expand current knowledge of the Gurney flap by supplementing previously gathered high-speed PIV data. The spatially coarser data from previous studies offered time-resolved flow information, while the current study provided smaller-scale information important for understanding the larger scale flow events.

D. R. Troolin, TSI Incorporated, 500 Cardigan Road, Shoreview, MN 55126, USA
E. K. Longmire, Department of Aerospace Engineering and Mechanics, University of Minnesota, Minneapolis, MN 55455, USA

Future work will focus on exploring the Reynolds number effects more thoroughly. In particular, the upstream boundary layer thickness will be determined accurately, with the aim of understanding the importance of the Gurney flap height as it relates to the boundary layer thickness.

Acknowledgements
Special thanks to the University of Minnesota Aerospace Engineering and Mechanics Department for the use of the facilities and fabrication of the airfoil test sections.

5
References

Blake W (1986) Mechanics of Flow-Induced Sound and Vibration Vol. II, Academic Press, Inc., pp. 756-782.
Jeffrey D; Zhang X; Hurst D (2000) Aerodynamics of Gurney Flaps on a Single-Element High-Lift Wing, Journal of Aircraft, Vol. 37. No. 2, pp. 295-301.
Liebeck R (1978) Design of subsonic airfoils for high lift. Journal of Aircraft 15(9), pp. 547-61.
Neuhart D; Pendergraft O (1988) A water tunnel study of Gurney flaps. NASA TM 4071.
Troolin, D. R., Longmire, E.K., and Lai, W.T. (2006a) "Time-resolved PIV analysis of flow over a NACA 0015 airfoil with Gurney flap," *Experiments in Fluids*, **41**, 241-254.
Troolin D; Longmire E; Lai W (2006b) "The Effect of Gurney Flap Height on Vortex Shedding Modes Behind Symmetric Airfoils," *13th Int. Symp. on Applications of Laser Techniques to Fluid Mechanics,* Lisbon, Portugal, 26-29 June, 2006.
Wadcock A (1987) Investigations of low-speed turbulent separated flow around airfoils. NASA CR 177450.
Wereley S; Gui L (2001) PIV measurement in a four-roll-mill flow with a central difference image correction (CDIC) method, 4th International Symposium on Particle Image Velocimetry, Göttingen, Germany, September 17.

D. R. Troolin, TSI Incorporated, 500 Cardigan Road, Shoreview, MN 55126, USA
E. K. Longmire, Department of Aerospace Engineering and Mechanics, University of Minnesota, Minneapolis, MN 55455, USA